AIAA SciTech Forum
4-8 January 2016, San Diego, California, USA
54th AIAA Aerospace Sciences Meeting

10.2514/6.2016-1249



# Simulation of $O_2$–N Collisions on *ab-initio* Potential Energy Surfaces

Daniil A. Andrienko*

Iain D. Boyd †

*Department of Aerospace Engineering, University of Michigan, Ann Arbor, MI, 48109*



**Investigation of $O_2$-N collisions is performed by means of the Quasi-Classical Trajectory method on the two lowest *ab-initio* potential energy surfaces. A complete set of bound-bound and bound-free transition rates is obtained for each precollisional rovibrational state. Special attention is paid to the vibrational and rotational relaxation of oxygen as a result of chemically non-reactive interaction with nitrogen atoms. It is found that the vibrational relaxation of oxygen occurs via the formation of an intermediate $NO_2$ complex with a large number of mutual internuclear vibrations before the final departure of the projectiles. The efficient energy randomization results in rapid vibrational relaxation at low temperatures, compared to other molecular systems with a purely repulsive potential. The vibrational relaxation time, computed by means of master equation studies, is nearly an order of magnitude lower than the relaxation time in $N_2$-O collisions. The rotational nonequilibrium starts to play a significant effect at translational temperatures above 8000 K. The present work provides convenient relations for the vibrational and rotational relaxation times as well as for the quasi-steady dissociation rate coefficient and thus fills the gap in data due to a lack of experimental measurements for this system.**

## I. Introduction

The interaction of oxygen molecules with nitrogen atoms is important in shock heated air, the chemistry of the upper atmosphere, and the combustion of carbon-based fuels. The formation of nitric oxide in these applications occurs via the Zeldovich mechanism [1]

$$\mathrm{O}_2\left(X^3\Sigma_g^-\right) + \mathrm{N}\left({}^4S\right) \rightarrow \mathrm{NO}\left(X^2\Pi\right) + \mathrm{O}\left({}^3P\right). \tag{1}$$

It is well known that the product of reaction (1) has a strong non-Boltzmann distribution of vibrational quanta [2–4]. The rate of reaction (1) as well as the process of NO quenching by molecular oxygen set a background for the explanation of infrared chemiluminescence in the upper atmosphere. A considerable amount of work [5, 6], besides that already mentioned, has been devoted to the study of the Zeldovich mechanism.

However, the $O_2$–N nonreactive channel of the interaction can also be important in modeling flows with a large number of nitrogen atoms. State-specific data on $O_2$–N collisions becomes necessary when attempting to develop high fidelity thermochemistry models of nonequilibrium hypersonic flows. During the past decade, a significant amount of work dealing with the state-resolved chemistry of nitrogen has been conducted [4, 7, 8]. The chemistry of molecular oxygen is studied less often, mainly due to the relatively rapid $O_2$ dissociation in hypersonic flows, generated during the reentry of spacecraft. However, a significant amount of oxygen is encountered during the flight of hypersonic vehicles at moderate velocity. Meanwhile, to the authors' knowledge, a model of oxygen relaxation in collisions with nitrogen atoms has not been proposed yet. Taking these facts into account, it is of interest to revisit the following reactions

$$\mathrm{O}_2\left(X^3\Sigma_g^-\right)(v_i, j_i) + \mathrm{N}\left({}^4S\right) \rightarrow \mathrm{O}_2\left(X^3\Sigma_g^-\right)(v_f, j_f) + \mathrm{N}\left({}^4S\right) \tag{2}$$

*Postdoctoral research fellow, Department of Aerospace Engineering, University of Michigan, 1320 Beal Ave
†James E. Knott Professor, Department of Aerospace Engineering, University of Michigan, 1320 Beal Ave

$$O_2\left(X^3\Sigma_g^-\right)(v_i, j_i) + N\left(^4S\right) \rightarrow O\left(^3P\right) + O\left(^3P\right) + N\left(^4S\right) \quad (3)$$

using the most recent theoretical data. The experimental study of the $O_2$–N system is complicated due to the large difference in dissociation energies of oxygen and nitrogen molecules. The presence of fast chemical reactions involving nitric oxide also complicates measurements of the vibrational distribution of products. As a result, experimental data on oxygen relaxation in $O_2$–N collisions is absent. To overcome this difficulty, an equality of relaxation times in $O_2$–N and $N_2$–O collisions has been assumed in computational models of hypersonic flows [9]. While this assumption can be partially justified due to the similar masses of reactants, state-to-state reaction rates are desirable for the implementation of more accurate state-resolved models of hypersonic flows.

The present work adopts two recently generated $2A'$ and $4A'$ potential energy surfaces (PESs) based on the *ab-initio* calculations of a large number of points in the $C_s$ and $C_{2v}$ configurations [10] of the $NO_2$ molecular system. These new PESs provide accurate curve fitted relations for over 1500 and 900 *ab-initio* points, respectively; and more realistic values of the potential barrier compared to previously reported data [5].

This paper is organized as follows. Section II describes the basic properties of the potential energy surfaces and addresses the governing equations of the QCT method and kinetic equations. Section III consists of multiple subsections and discusses the results of the present study. Subsection A compares the present thermal relaxation rates with those previously reported in the literature. Subsection B presents the study of microscopic parameters of trajectories. Subsection C provides the discussion on the state-resolved population of the rovibrational manifold during thermalization to equilibrium conditions. Subsection D discusses the specifics of vibrational and rotational relaxation. Subsection E presents the results on coupling of thermal relaxation with the depletion mechanism of oxygen in a bath of nitrogen atoms. Conclusions are drawn in Section IV.

## II. Methodology

### A. Potential energy surface

The Zeldovich mechanism proceeds via the two lowest $2A'$ and $4A'$ potential energy surfaces. The experimentally measured potential barriers of these PESs are 0.355 and 0.694 eV, respectively. At temperatures below 5,000 K, collisions of molecular oxygen with atomic nitrogen proceed on the ground $2A'$ PES, while at higher temperatures, observed in hypersonic flows, it is important to account for both of the $2A'$ and $4A'$ PES contributions. The $O_2$–N collisions, that induce the bound-bound transition of oxygen (nonreactive channel), also occur on the excited $6A'$ potential energy surface. However, it is expected that the contribution of this PES is small in the range of temperatures from 1,000 to 15,000 K, due to the relatively high potential energy barrier. The $6A'$ PES correlates with the first excited electronic state $NO\left(a^4\Pi\right)$ with an energy of 4.8 eV above the ground configuration. Because an analytical form of the $6A'$ PES is not yet proposed in the literature, the investigation of $O_2$–N collisions is performed only taking into account the $2A'$ and $4A'$ PESs in the range of low to moderate temperatures. One should note that, since $2A'$ and $4A'$ PESs do not correlate with excited states of the oxygen molecule, the results should be considered accurate for the entire temperature range reported in the present work.

The equipotential curves of the $2A'$ and $4A'$ surfaces by Sayós et al. [10] are shown in Figs. 1a and 2a, respectively. The angles between the O–O and N–O bonds are set to 115° and 109.4° that correspond to the location of a saddle point. Note, that the $2A'$ PES correlates with $NO_2\left(X^2A_1\right)$. The $2A'$ and $4A'$ PESs have potential barriers of 0.299 and 0.557 eV, respectively, which appears to be the closest agreement to the experimental data. For reference, the equipotential levels of $2A'$ and $4A'$ PESs generated by Bose and Candler [4] are shown in Fig. 1b and 2b for the same N–O–O angle. One can see some differences in these two sets of potential energy surfaces at small values of intermolecular distance. Also, both the $2A'$ and $4A'$ PESs by Sayós et al. demonstrate less pronounced attractive properties compared to [4], as follows from the behavior of contours at the same equipotential level. It will be shown later that these facts lead to some differences in results, especially at high temperatures.

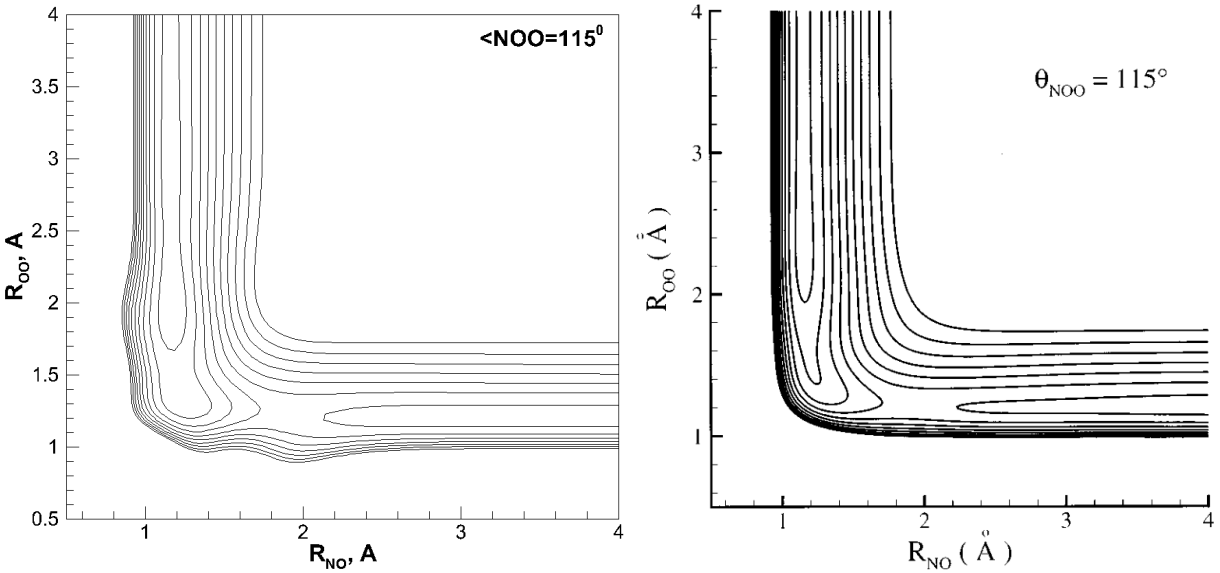


(a) Sayós et al. [10]

(b) Curve fit of [5] by Bose and Candler [4]

Fig. 1: 2A′ Potential energy surface, N–O–O angle is fixed at the *ab-initio* saddle point configuration

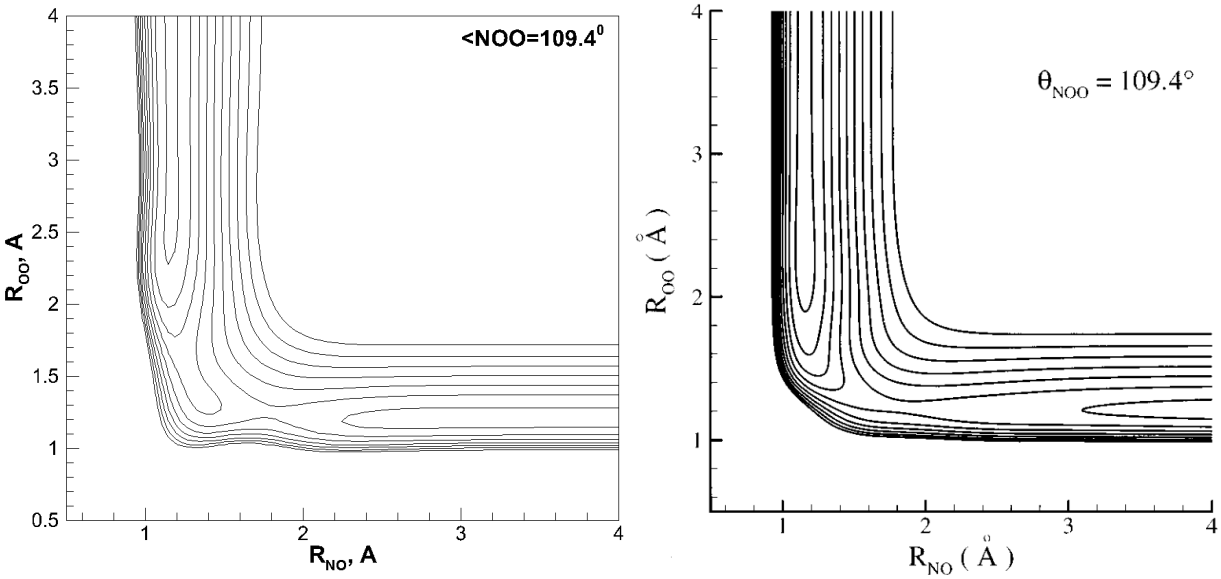


(a) Sayós et al. [10]

(b) Curve fit of [5] by Bose and Candler [4]

Fig. 2: 4A′ Potential energy surface, N–O–O angle is fixed at the *ab-initio* saddle point configuration

## B. QCT method

In the present work, the Quasi Classical Trajectory (QCT) method is used to generate vibrationally-resolved transition cross sections of reactions (1) - (3). The initial rovibrational state, $(v_i, j_i)$, is fixed in each batch of trajectories. The internuclear separation in the isolated oxygen molecule is initialized by the random sampling of oscillation phase based on the period of vibrational motion. Initial separation of the target and projectile particles is given by 15 $\mathring{A}$. Hamilton's differential equations, described in [11], are solved by the Adams-Moulton method of $11^{\text{th}}$ order of accuracy. The impact parameter, $b$, is sampled with a step size of 0.1 $\mathring{A}$. Every batch contains $2{\times}10^3$ trajectories. Analysis of the final state is performed according to [12]. Each trajectory is integrated with an error in the total energy not exceeding $10^{-4}$% A trajectory is terminated after the distance between products exceeds the initial separation. Each such trajectory is then classified into one of three possible channels: non-reactive bound-bound transition, exchange reaction, or dissociation (bound-free transition). The probability, $\Phi$, of the state-specific transition $(v_i, j_i) \rightarrow (v_f, j_f)$, where $(v_f, j_f)$ is the final rovibrational state, at a given collision energy $\mathrm{E}_{col}$ , is defined as follows:

$$\Phi\left(E_{col}\right) = \frac{2}{b_{max}^2} \int_0^{b_{max}} \left( \frac{N_{v_i j_i \rightarrow v_f j_f}}{N} \right) b db, \tag{4}$$

where $b_{max}$ is the impact parameter at which only elastic collisions are observed, $N_{v_i j_i \rightarrow v_f j_f}$ and $N$ are the number of trajectories with the desired transition and the total number of trajectories in the current batch of impact parameter, respectively. The probability of the bound-free transition is calculated in a manner similar to Eq. (4). The cross section of either bound-bound or bound-free transition is calculated as follows:

$$\sigma\left(E_{col}, v_i, j_i\right) = \pi b_{max}^2 \Phi\left(E_{col}, v_i, j_i\right), \tag{5}$$

where $\Phi$ is sampled over the five variables mentioned in Eq. (5): impact parameter $b$, initial azimuthal $\theta$ and polar $\phi$ orientations of the target molecule, initial orientation of the target molecule angular momentum $\eta$ and initial vibrational phase $\xi$ of the target molecule. The reaction probability is also defined by the final rovibrational state as well as by the channel of interest. The present calculations study dynamics of $O_2$–N collisions in the range of collision energy from 0.01 to 18 eV. This range is covered by 35 intervals of uneven length. Stratified sampling of the impact parameter is adopted to increase accuracy of statistical modeling. The procedure of trajectory simulation is repeated individually on the $2A'$ and $4A'$ PESs. The overall number of trajectories included in statistics is approximately $1.2{\times}10^{10}$ for each surface.

The present paper features the analysis of rates assuming trans-rotational equilibrium, as well as treating vibrational and rotational modes in a similar manner. As a first step in the analysis of the reaction rate dataset, trans-rotational equilibrium is assumed. In order to do so, the cross section of transition from the initial state to any final rotational state of the final vibrational level is computed as follows:

$$\sigma\left(E_{col}, v_i, j_i \rightarrow v_f\right) = \sum_{j_f} \sigma\left(E_{col}, v_i, j_i \rightarrow v_f, j_f\right). \tag{6}$$

The rate of either bound–bound or bound-free transition at the gas temperature $T$ is calculated by integrating the corresponding cross sections:

$$K\left(v_i, j_i, T\right) = \frac{8\pi}{\sqrt{\mu_{\mathrm{N,O_2}}}} \left(2\pi k_B T\right)^{-3/2} \int_0^{\infty} \sigma\left(E_{col}, v_i, j_i\right) E_{col} exp\left( \frac{-E_{col}}{k_B T} \right) dE_{col}. \tag{7}$$

For further analysis, it is convenient to average the reaction rate over all rotational levels that belong to the initial vibrational state. The averaging procedure assumes that each rotational level $j_i$ contributes to the rate according to the Boltzmann factor $w$:

$$w\left(j_i\right) = \epsilon g_e \left(2j_i + 1\right) exp\left(-\left(e_{v_i,j_i} - e_{v_i,0}\right)/k_B T\right), \tag{8}$$

where $\epsilon$ is the symmetry factor of $O_2$, and $g_e$ is the degeneracy of the electronic state. The Boltzmann-averaged rates of the bound-bound $(\nu_i \rightarrow \nu_f)$ and bound–free $(\nu_i \rightarrow c)$ transitions are derived using Eqs. (9) and (10):

$$K_{v_i \to v_f} = \frac{\sum_{j_i} \left( w_{j_i} \sum_{j_f} K_{v_i, j_i \to v_f, j_f} \right)}{\sum_{j_i} w_{j_i}}; \tag{9}$$

$$K_{v_i \to c} = \frac{\sum_{j_i} w_{j_i} K_{v_i, j_i \to c}}{\sum_{j_i} w_{j_i}}. \tag{10}$$

### C. Master equations studies

The rates of rovibrational transitions are incorporated into the system of master equations in order to describe thermalization of internal degrees of freedom toward the equilibrium state. The present approach considers thermal relaxation for each rovibrational state as well as assuming the presence of rotational equilibrium. For the latter, the system of master equations is formulated for each vibrational state. The state-specific dissociation and recombination are included in the present formulation unless the opposite is stated. The quasi-bound (QB) states are assumed to have an infinite lifetime. Solution of master equations is obtained for translational temperatures between 500 and 20,000 K. The resulting system of equations for the number density of rovibrational level $i$ can be written as follows:

$$\frac{dn_i}{dt} = \sum_{f \neq i} \left( K\left(T, v_i, j_i \to v_f, j_f\right) n_N n_f - K\left(T, v_f, j_f \to v_i, j_i\right) n_N n_i \right) + R\left(T, v_f, j_f\right) n_N n_O^2 - D\left(T, v_i, j_i\right) n_N n_i, \;\; i = 1...N_s, \;\; f = 1...N_s, \tag{11}$$

where $N_s$ is the total number of rovibrational states. The rates of bound-bound transitions are given by Eq. (7). Equation (11) describes the trans-rotational-vibrational energy transfer and is termed as the RVT thermodynamic model. An implicit method of third order accuracy for diagonal and second order accuracy for off-diagonal elements is applied to integrate Eq. (11). The initial number density, given by $n_{O_2,0} + n_{N,0}$, is set to $1{\times}10^{18}$ cm$^{-3}$. This is equivalent to a pressure of 1.3626 Atm at a gas temperature of 10,000 K. No mass exchange with the surrounding medium is allowed. To simulate conditions when the atom-molecule collisions are dominant, the initial number density of atomic oxygen is set to $\alpha$=0.99 of the total number density, if the opposite is not stated. At initial nonequilibrium conditions, the population of rovibrational states is given by the Boltzmann distribution with the temperature $T_0 = 100$ K, as follows from Eq. (12):

$$n_{i,0} = \frac{Q_i\left(T_{rot}, T_{vib}\right)}{\sum_i Q_i\left(T_{rot}, T_{vib}\right)} n_{O_2,0}, \tag{12}$$

where $Q_i\left(T_{rot}, T_{vib}\right) = \left(2j_i + 1\right) exp\left[-\left(e_{v_i,j_i} - e_{v_i,0}\right)/k_B T_{rot}\right] exp\left[-e_{v_i,0}/k_B T_{vib}\right]$ is the two-temperature rovibrational partition function, and $n_{O_2,0}$ is the total number density of oxygen. The initial internal temperatures, $T_{rot,0}$ and $T_{vib,0}$, are equal to $T_0$ when the RVT model is applied.

The system of governing equations in the case of trans-rotational equilibrium has the following appearance:

$$\frac{dn_i}{dt} = \sum_{f \neq i} \left( K\left(T, v_f \to v_i\right) n_O n_f - K\left(T, v_i, \to v_f\right) n_O n_i \right) + R\left(T, v_f\right) n_N n_O^2 - D\left(T, v_i\right) n_N n_i, i = 1...N_v, \;\; f = 1...N_v, \tag{13}$$

where $N_v$ is the total number of vibrational states, $D$ and $R$ are the dissociation and recombination rate coefficients. Equation (13) describes the trans-vibrational energy transfer and is termed as the VT model. The initial rotational temperature is set to the heat bath temperature, and the initial vibrational temperature is set to $T_0$.

# III. Results

## A. Verification of results

The variation of the cross section of reaction (1) with the energy of collision, is shown in Fig. 3 for initial state $O_2$ ($v_i = 0, j_i = 7$) and ($v_i = 0, j_i = 9$). The present data is compared to the results by Bose and Candler and by Gilibert et al. [13], given for the rovibrational state $O_2$ ($v_i = 0, j_i = 8$). It is impossible to perform a direct comparison since in the original works all rotational states of molecular oxygen were taken into account, while the quantum-mechanical rules of nuclear spin statistics [14] dictate the absence of the even-numbered rotational states of oxygen due to zero nuclear spin.

In Fig. 3, the square symbols and solid line correspond to the present results obtained on the 2A′ PES for $j_i = 7$ and 9, respectively. The red dashed and blue dashed-dotted lines correspond to the data by [4] and [13], respectively. The present calculations confirm the lower potential energy barrier of 2A′ PES [10], compared to previously reported data. The difference in the cross sections increases at high collision energies. This can be explained by some disagreements in the PESs, shown in Figs. 1a and 1b, in the region of small internuclear distances, inaccessible at small collision energies. At higher collision energies, the present results are in agreement with the work by Gilibert et al. which used the same *ab-initio* data by Jaffe et al. [5] with a different curve fit technique. As discussed in [4], the PES by Gilibert et al. indeed introduces an undesirable artificial potential barrier, however its presence seems to be unimportant at high collision energies. For reference, the cross section of reaction (1) on the 4A′ PES, shown by the dashed black line, is considerably smaller than that on the 2A′ PES and has a higher threshold energy of channel opening.

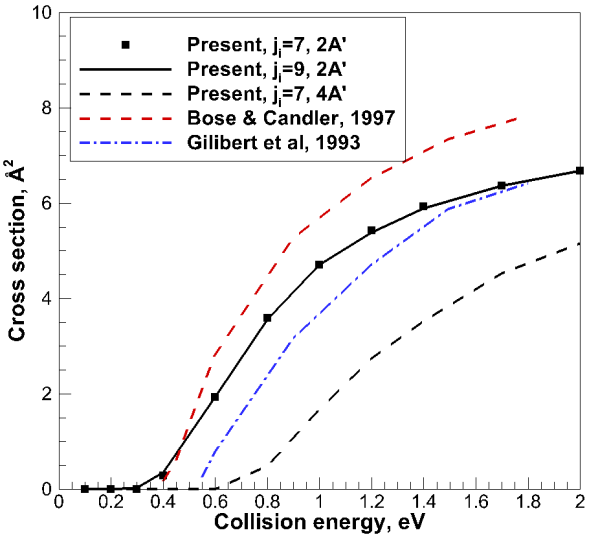


Fig. 3: Integral cross section of transition $O_2$ ($v_i = 0, j_i$) +N → NO + N, $j_i$=7 and 9

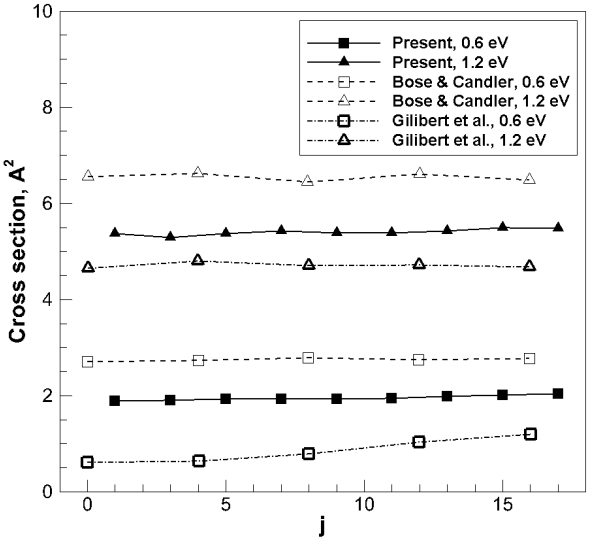


Fig. 4: Variation of cross section of $O_2$ ($v_i = 0, j_i$) +N → NO + N reaction, $j_i$=1 ... 17

The variation of cross section of reaction (1) with the initial rotational quantum number is shown in Fig. 4 at collisional energies of 0.6 and 1.2 eV on the 2A′ PES. As one can see, the present data has intermediate values between the results reported in [4] and [13]. At these conditions, the initial rotational energy of reactants has no significant influence on the cross section of the Zeldovich mechanism, since the collisional energy is significantly larger than the potential barrier. At the low collision energy of 0.6 eV, the present data is closer to the work by Bose and Candler, while at the energy of 1.2 eV, the present cross section is noticeably smaller than the latter.

Lastly, the vibrationally-resolved rate of the Zeldovich reaction is shown in Fig. 5 in the range of trans-rotational temperature between 1,000 and 14,000 K. The black dashed and solid lines correspond to the present results for $v_i = 0$ and 1, respectively. These results include the contribution from both the 2A′ and 4A′ PESs. Results by Bose and Candler are shown with rectangular and delta symbols. Additionally, the individual contributions of the 2A′ and 4A′ PESs are represented by red solid and dashed curves. The present comparison shows a good agreement between two independent simulations on two different sets of potential energy surfaces. While some disagreement is observed in more detailed study, highly averaged parameters,

such as the rotationally-averaged reaction rate, shows a relatively small sensitivity to the computational details. It is interesting to note that the contribution of the 4A′ PES becomes dominant at a temperature of 4,000 K and higher, which may be caused by the larger contribution of this PES at highly excited initial rotational states of the reactant.

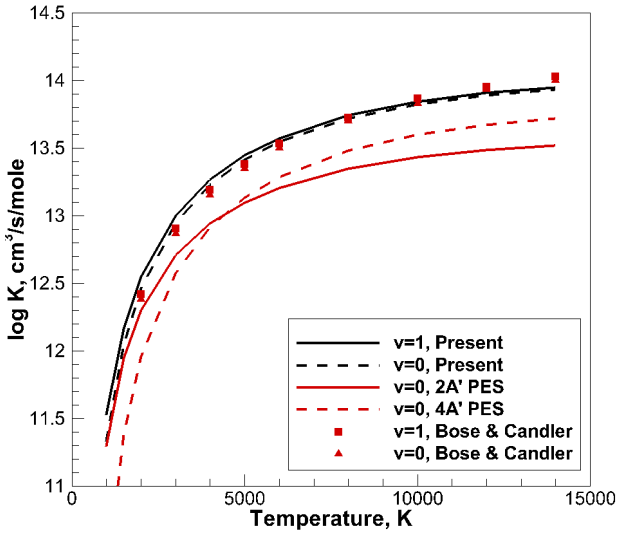


Fig. 5: Variation of $O_2$ ($\nu_i = 0$) +N → NO + N, reaction rate with trans-rotational temperature

Vibrationally resolved rates of $O_2$–N non-reactive and exchange collisions are shown in Figs. 6 and 7, respectively. In these calculations, the rotational spectrum of rates is averaged at $T_{rot} = T$. The rates of mono- and multiquantum vibrational deactivation are strongly dependent on the potential energy surface, as follows from Fig. 6. The energy randomization in collisions that follow the 2A′ PES occurs more efficiently than for the 4A′ PES. For the former, the rates of deactivation from $v_i = 10$ depend weakly on temperature, while for the latter, the deactivation proceeds much slower at low temperatures.

There are also some differences in the final vibrational state of NO between the 2A′ and 4A′ surfaces. At translational temperature of 3000 K, the exchange channel is more probable for 2A′ PES, as can be judged by the appearance of the solid curves in Fig. 7. However, the rate of production of NO($v_f = 13$) from $O_2$ ($v_i = 10$) via 4A′ is higher than NO($v_f = 10$). At higher temperatures, the situation is opposite: the 4A′ PES is more efficient in generating excited states of nitric oxide than the 2A′ PES. The temperature dependences of rates for 10,000 and 16,000 K are similar for both PESs, indicating that the influence of the potential barrier is small at these conditions.

## B. Microscopic parameters of trajectories

To gain insight into the process of vibrational relaxation, mutual permutations of nuclei and energy randomization in $O_2$–N collisions are studied in detail. Following the work of Lee et al. [15], the simulation of each collision is carried out tracking the number of exchanges in the shortest interatomic distance (NESID). This parameter is calculated by analyzing the distance between each pair of atoms. When the projectile atom A and target molecule BC are significantly separated from each other, the minimal interatomic distance is $R_{BC}$. When the atom approaches the molecule, one can expect that at some point, the minimal interatomic distance may become either $R_{AC}$ or $R_{AB}$. If this happens, the shortest interatomic distance is reassigned and the NESID value is increased by unity. The NESID can be equal to zero, indicating that the projectile atom approached the molecule with the minimum of interaction. A high value of NESID corresponds to intense intermolecular energy transfer, as will be shown later. It is worth to note that the NESID parameter is a meaningful characteristic only for collisions with a target and projectile molecule attracted to each other. For systems with a repulsive potential, such as $O_2$–Ar, the NESID value is always zero.

In the present work, the NESID is calculated for the high-lying initial rovibrational state $\nu_i$=20, $j_i$=1. Figures 8a - 8c reflect the number of mutual permutations of nuclei for the 2A′ PES at collision energies of 0.6, 1, 2 and 4 eV. The vibrationally inelastic channel demonstrates a relatively weak dependence of NESID

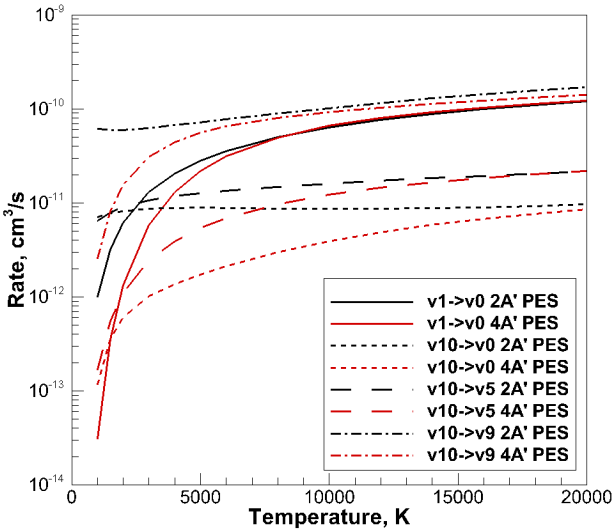


Fig. 6: Rates of $O_2\,(\nu_i)$ +N $\rightarrow$ $O_2\,(\nu_f)$ + N

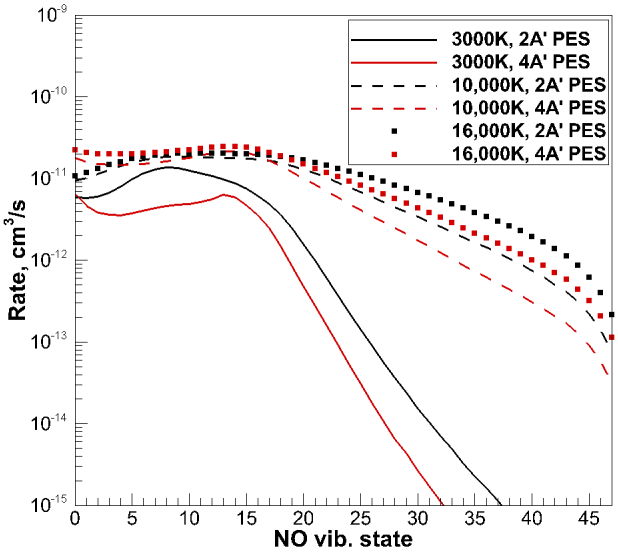


Fig. 7: Rates of $O_2\,(\nu_i = 10)$ +N $\rightarrow$ NO($\nu_f$) + O, at T=3000, 10,000 and 16,000K

on the kinetic energy, although trajectories with NESID larger than 6 are present only at low energetic collisions. The situation is entirely different for the vibrational deactivation and in the case of nitrogen atom insertion. In both cases, the number of trajectories with non-zero NESID is substantially larger, compared to that in Fig. 8a. Moreover, the dependence of NESID on the collisional energy can be clearly seen: at low $E_{col}$ the nitrogen atom has a large probability to be trapped into an oscillatory motion with the oxygen molecule. The product of this interaction can result in the formation of nitric oxide with a strongly non-Boltzmann distribution of vibrational quanta [13]. Clearly, such an efficient energy transformation is owing to the large potential well of -8.96 eV of the 2A′ PES that correlates with the formation of the $NO_2$ molecule.

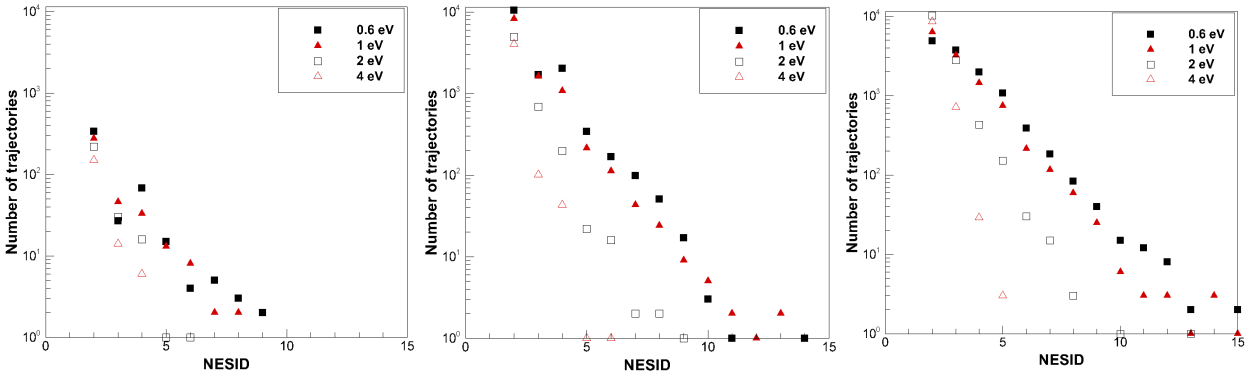


(a) nonreactive channel, $v_f = 20$ (b) nonreactive channel, $v_f < 20$ (c) exchange channel

Fig. 8: NESID, PES 2A′

The 4A′ PES possesses more repulsive properties and a higher potential barrier, compared to the 2A′ PES. The previously reported studies of macroscopic parameters of trajectories in systems with a strongly repulsive potential, such as $O_2$–Ar, revealed significantly less efficient energy transfer between translational and internal modes, compared to molecular systems with a large attractive component [16]. The present results confirm this observation by comparing the number of trajectories leading to either vibrational deactivation or exchange reaction between the 2A′ and 4A′ PESs. For the latter, a much weaker dependence of NESID on the collisional energy is observed, as follows from Figs. 9a - 9c.

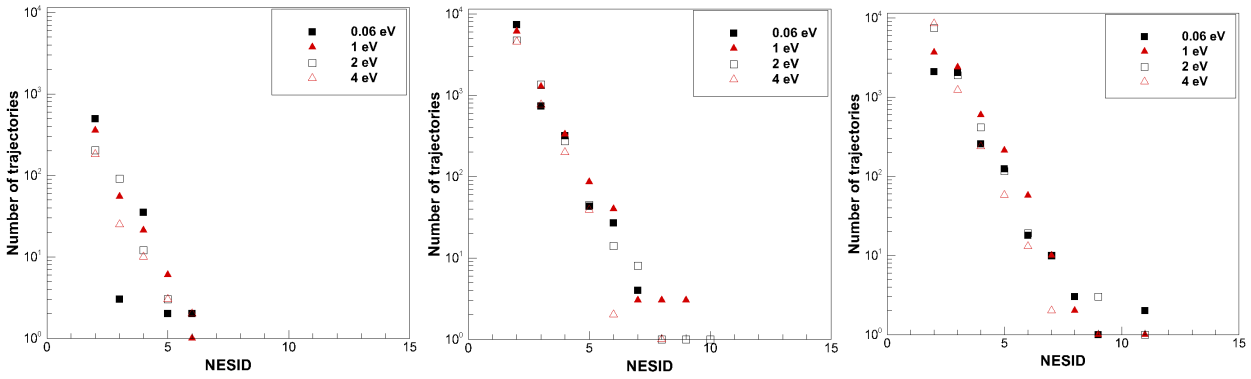


(a) nonreactive channel, $v_f = 20$ (b) nonreactive channel, $v_f < 20$ (c) exchange channel

Fig. 9: NESID, PES 4A′

### C. Population of the rovibrational ladder

The solution of master equations provides insight on the evolution of the rovibrational manifold during thermalization. By analyzing the rovibrational distribution function generated by $O_2$–N collisions on 2A′ and 4A′ surfaces, it is possible to judge about the influence of PES topographical features on the process of thermalization. In order to simplify the analysis, dissociation is artificially excluded from the simulations in this section. The population of the rovibrational ladder is presented in Fig. 10 for 2A′ and 4A′ PESs at translational temperatures of 5000 and 10,000 K.

At the early state of relaxation, the population of the ladder substantially differs from the equilibrium state, shown by the green symbols. When comparing the thermalization process between the two lowest $O_2N$ PESs, it is possible to see that in the case of 2A′ the scatter of the populations is noticeably smaller than that in the 4A′ PES. This is explained by higher rates of mono- and multi-quantum transitions, as follows from Fig. 6, and thus, more effective re-distribution of energy between internal states. One of possible reasons for this is the existence of the 2A′ potential well which results in effective "scrambling" of precollisional states. At the late stage of relaxation, the rovibrational manifold becomes depleted into separate strands, each of which corresponds to a particular vibrational state. Judging by the difference in the slope of these strands, it is possible to conclude that the rotational relaxation in collisions that follow the 2A′ PES occurs more rapidly than that for 4A′ PES at the considered translational temperatures.

### D. Vibrational and rotational relaxation times

Vibrational and rotational relaxation times characterize the rate of thermalization of the rovibrational manifold toward the equilibrium conditions. Using the energy transfer rates, generated in the present work, it is possible to obtain $O_2$–N $\tau_{vib}$ and $\tau_{rot}$ by solving the system of master equations and taking into account all relevant energy states and transitions, contributing to the relaxation. Such analysis is performed for 2A′ and 4A′ PESs individually, as well as considering them in a concurrent manner.

First, the situation when $T = T_{rot}$ is considered. Since the populations of $v = 0$ and $v = 1$ account for at least 90 % of the entire vibrational ladder for temperatures below 2,000 K, the two-state model provides important insight into the process of vibrational relaxation. The total cross section of monoquantum deactivation from rovibrational level $v_i = 1, j_i$ to $v_f = 0$, and any $j_f$ is obtained by utilizing Eq. (6). The rate of the process $(v_i, j_i) \to v_f$ is calculated using Eq. (7). The corresponding rate $K_{v_i,j_i \to v_f}$ is averaged over the initial rotational levels $j_i$, assuming $T_{rot} = T$, to obtain the rate of monoquantum deactivation $K_{1\to0}$. Then the two-state vibrational relaxation time is obtained as follows

$$P\tau_{vib} = \frac{k_B T}{K_{1\to0} - K_{0\to1}}. \tag{14}$$

At high temperatures, however, Eq. 14 fails to describe the relaxation of highly excited vibrational states. The e-folding method by Park [17] can be used to obtain $\tau_{rot}$ and $\tau_{vib}$. The relaxation times, derived from Eq. (14) and from the solution of master equations by the e-folding method, including rates from the 2A′

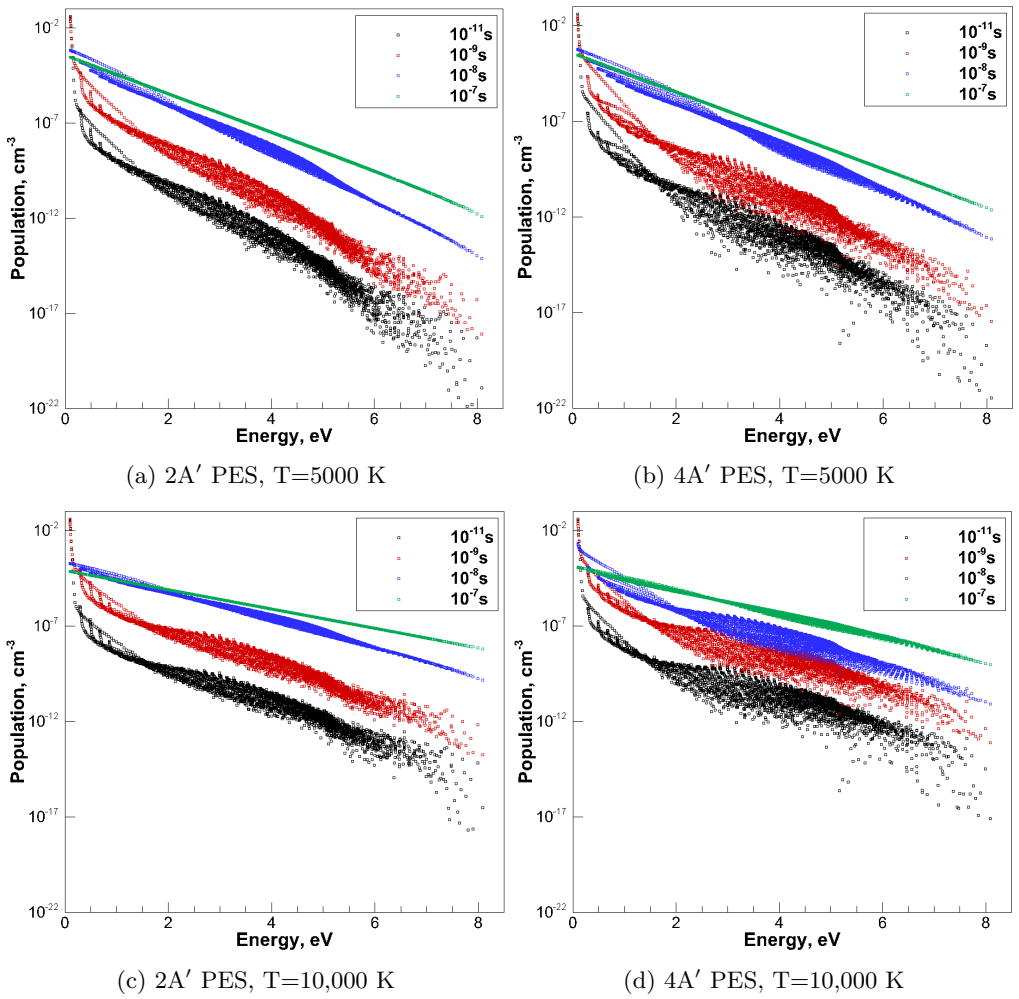


(a) 2A′ PES, T=5000 K

(b) 4A′ PES, T=5000 K

(c) 2A′ PES, T=10,000 K

(d) 4A′ PES, T=10,000 K

Fig. 10: Population of rovibrational ladder

and 4A′ PESs, are shown in Fig. 11a with unsymboled dashed and solid lines, respectively. The individual contributions of the 2A′ and 4A′ potential energy surfaces in Eq. (14) are shown by lines with square and delta symbols, respectively. The Millikan and White relaxation time, based on the reduced mass of the $O_2$–N system and the characteristic vibrational frequency of oxygen, $\omega_e = 1580.193$ cm$^{-1}$, is shown by the dashed-dotted line. Finally, the relaxation time in $N_2$–O collisions, obtained in [18–20] and used by Park [9] to model the $O_2$–N vibrational relaxation, is shown by the blue symbols.

The contribution of the lowest 2A′ PES on vibrational relaxation dominates at kinetic temperatures below 3000 K. At higher temperatures, the first excited PES governs the vibrational relaxation, while the contribution of the ground PES becomes small, but non-vanishing. A deviation of the relaxation time, derived by Eq. (14), from the e-folding relaxation time is observed for temperatures as low as 2,000 K. The present data for the $O_2$–N system shows satisfactory agreement with the $N_2$–O relaxation time only at low temperatures, while at high temperature the calculated $O_2$–N relaxation time is nearly an order of magnitude lower than that in $N_2$–O collisions. The Millikan-White equation strongly overestimates the vibrational relaxation time, showing an inadequacy of its utilization for collisions that involve multiple PESs with a deep minimum of potential energy.

Figure 11b presents the $O_2$–N vibrational and rotational relaxation times obtained by means of the e-folding method and the RVT thermodynamic model. The intermolecular attraction and the lower potential barrier of 2A′ PES results in much faster relaxation, compared to the 4A′ PES at low temperatures. However, at temperatures above 5000 K the relaxation via the 4A′ PES becomes more efficient than via the 2A′ PES. A similar effect was observed when relaxation in oxygen occurs via $O_2$–O and $O_2$–$O_2$ channels simultaneously

[21]. In that case, the repulsive interaction in pure $O_2$ is more efficient for vibrational thermalization at temperatures above 10,000 K, compared to the relaxation via the $O_3$ complex.

The assumption about rotational equilibrium in $O_2$–N collisions is valid for temperatures below 8000 K. Above this point, the vibrational and rotational modes should be treated in a concurrent manner. It is worth to note, that at very high temperatures (above 16,000 K), $\tau_{rot}$ exceeds $\tau_{vib}$ for both PESs. A possible explanation of this fact lays in the absence of the exchange channel in the $O_2$–N system. Similar behavior of relaxation times is observed for $N_2$–N [7], when the exchange channel is artificially excluded from the master equation simulation. The exchange channel is the efficient mechanism for scrambling of precollisional vibrational states, and, due to non-symmetry of the $O_2$–N system, such mechanism of thermalization is not available.

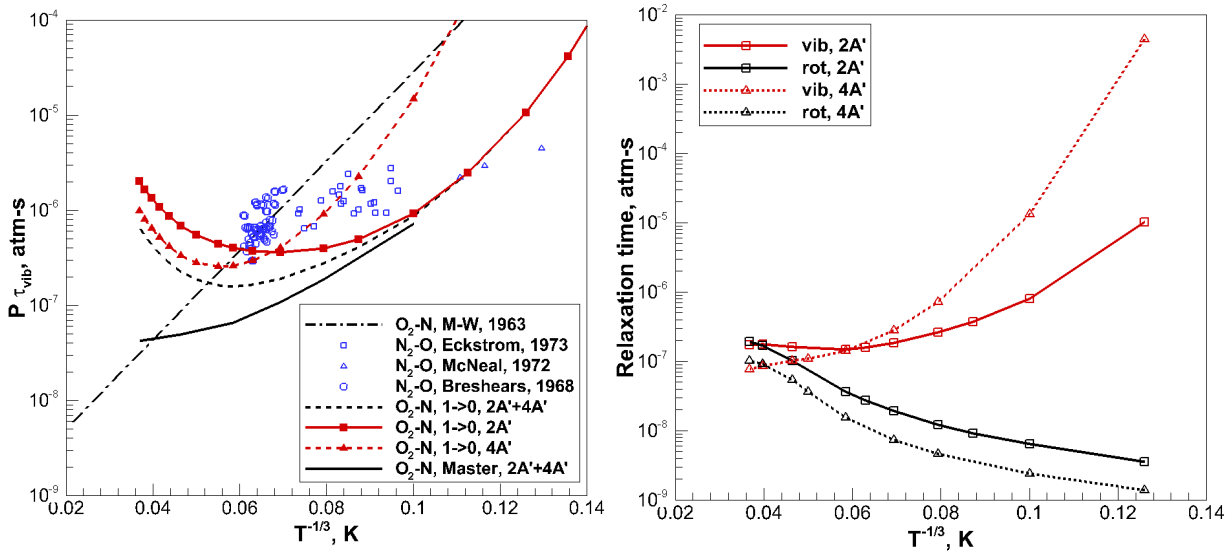


(a) $O_2$–N and $N_2$–O vibrational relaxation times, VT thermodynamic model

(b) Vibrational and rotational relaxation times, RVT thermodynamic model

Fig. 11: Vibrational relaxation time

A comparison of $O_2$ vibrational relaxation times in collisions with different projectiles, obtained via the QCT method and master equation simulation, is shown in Fig. 12. Square symbols correspond to $O_2$–N, triangular and circular symbols describe the data on $O_2$–O [16] and $O_2$–Ar [22], respectively. In the range of moderate to low temperatures, the fastest relaxation time is observed in the $O_2$–O system. This is due to the strong attractive component in the PES of the ozone molecule [23]. The energy randomization between target and projectile in the $O_3$ complex is so efficient that the relaxation time decreases with temperature, since the probability of vibrational transition is smaller for highly energetic collisions.

On the contrary, a system with a strongly repulsive potential, such as $O_2$–Ar, demonstrates the typical Millikan-White behavior of the relaxation time, which can be fit by a linear dependence in the $P\tau$–$T^{-1/3}$ coordinates. At high kinetic temperatures, the principles of Landau-Teller theory break down, which leads to the deviation of the relaxation time from the linear dependence. The temperature dependence of the vibrational relaxation time in $O_2$–N collisions demonstrates the behavior of a molecular system with a large repulsive component in the PES, which becomes important at high energies. At low temperatures, the $O_2$–N relaxation time is several orders of magnitude lower than that in the purely repulsive molecular system, which confirms the importance of the PES with a low potential barrier and a deep minimum of $NO_2$ $\left(X^2A_1\right)$ formation for the process of vibrational relaxation.

### E. Thermal relaxation in the presence of dissociation

The system of master equations, coupled to the set of bound-bound and bound-free transition rates, provides a convenient tool for the study of coupled $O_2$ relaxation-dissociation mechanisms in the heat bath of nitrogen atoms. Following this approach, it is possible to study the validity of the QSS assumption for

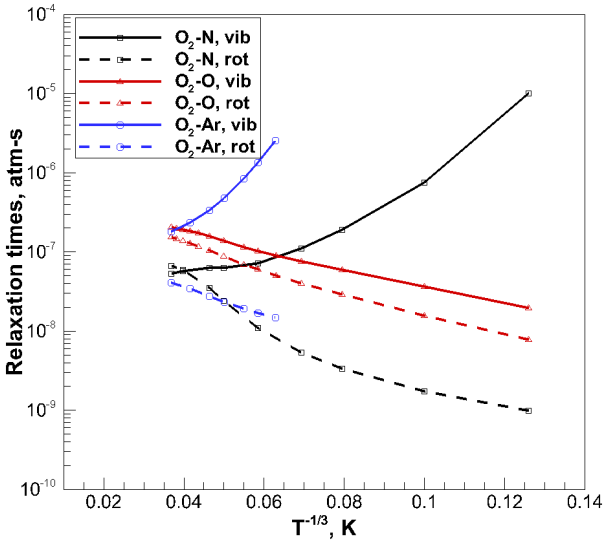


Fig. 12: Comparison of $O_2$–N, $O_2$-Ar and $O_2$-O systems

two different PESs and derive the quasi-steady dissociation rate coefficient and the average loss of internal energy during the phase of active chemical transformations. The variation of $O_2$ vibrational and rotational temperatures is shown in Figs. 13a and 13b for $2A'$ and $4A'$ PESs, respectively. In these simulations, the total number density of particles is set to $10^{18}$ cm$^{-3}$ with 5 % molar fraction of nitrogen atoms. No atomic oxygen is introduced initially. The RVT thermodynamic model is considered.

For temperatures below 8000 K, thermal relaxation occurs prior to the onset of dissociation. At these conditions, the $O_2$ depletion does not take place immediately after the rotational mode is thermalized, but when the vibrational equilibrium occurs. This means that the dissociation preferentially occurs from higher vibrational and lower rotational states at low temperatures. With the translational temperature increasing further, the quasi-steady internal temperatures deviate from the equilibrium level, since the rates of dissociation and thermal relaxation become comparable. Only a small amount of atomic oxygen is generated prior to the QSS phase at temperatures of 8000 and 10,000 K, indicating the validity of the QSS assumption at these conditions. However, at T=16,000 K, nearly half of the oxygen molecules have already dissociated prior to the QSS phase, which indicates breakdown of the QSS theory. This conclusion can be made for both PESs.

The rovibrational thermalization via concurrent relaxation on the $2A'$ and $4A'$ PESs is shown in Fig. 14. The quasi-steady vibrational and rotational temperatures monotonically increase at low T, eventually reaching the constant level. This level is just below the value of 10,000 K. At high temperatures, the vibrational and rotational temperatures closely follow each other. In this case, reduced order modeling of $O_2$–N thermalization can be performed using a unified internal temperature that describes the distribution of both vibrational and rotational degrees of freedom. The information about $T_{vib}$ during the QSS phase can be used for verification of dissociation rates in the presence of vibrational nonequilibrium, proposed in the literature [24, 25].

Thermalization of the vibrational mode assuming rotational equilibrium is shown in Fig. 15. Profiles of vibrational temperature are shown with solid and dashed lines for the $2A'$ and $4A'$ PESs, respectively. In the temperature interval between 3000 and 8000 K, the relaxation on these two PESs proceeds in a similar manner. At higher temperatures, however, there are some apparent differences. While the QSS vibrational temperature increases monotonically for collisions that proceed on the $4A'$ PES, the quasi-stationary $T_{vib}$ for the $2A'$ PES experiences a maximum at T=16,000 K. A similar effect was observed for $O_2$ state-resolved relaxation in collisions with parent atom [21]. In the $O_2$–O interaction, the atom-molecular collisions proceed on a barrierless PES that has a minimum of $O_3$ metastable formation. In that case, the maximum of quasi-steady vibrational temperature is observed for translational temperatures of approximately 10,000 K. It is worth to note that the QSS vibrational temperature is lower when rotational equilibrium is assumed, since the vibrational relaxation time in this case is shorter compared to that in the model of rovibrational thermal

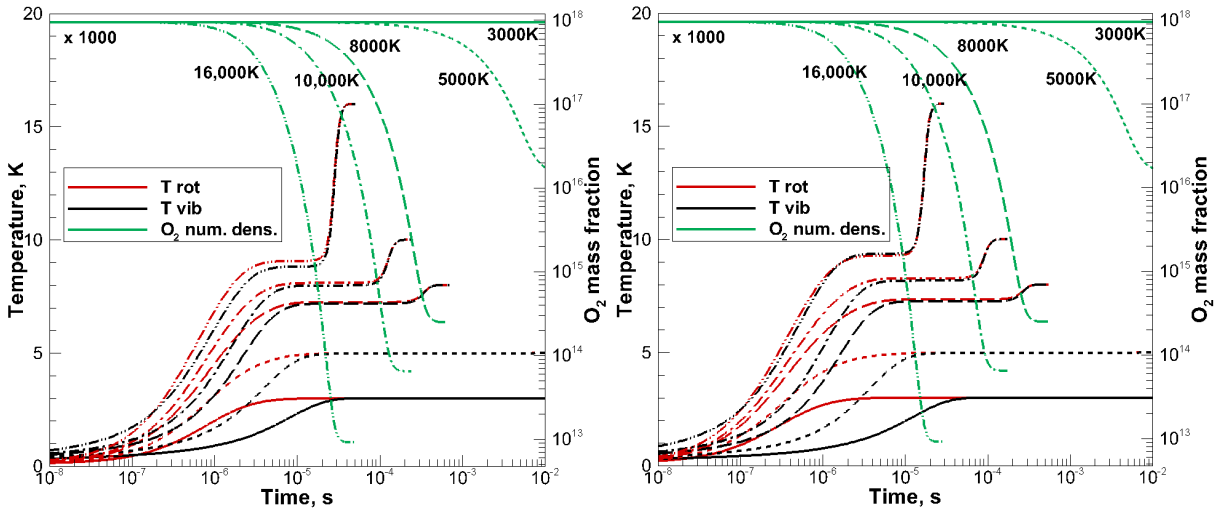


(a) PES 2A′ (b) PES 4A′

Fig. 13: $\tau_{vib}$, $\tau_{rot}$ and $O_2$ number density in the presence of dissociation/recombination reactions.

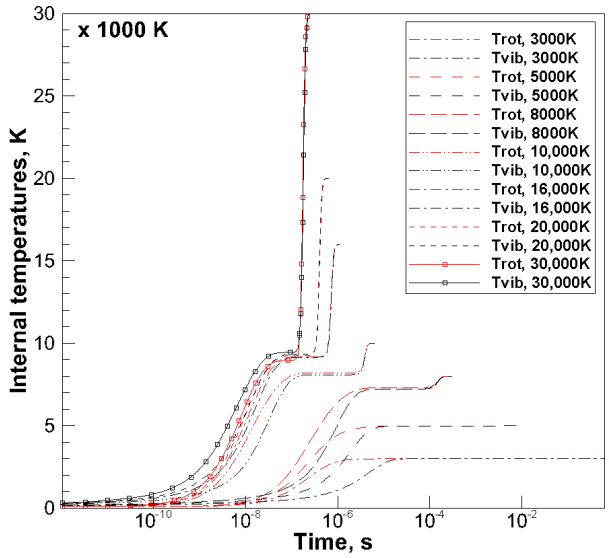


Fig. 14: Rovibrational thermalization via 2A′ and 4A′ PESs

relaxation, as follows from Fig. 16.

In order to describe the coupling between the processes of rovibrational relaxation and dissociation, it is convenient to define the energy rate constants, that describe the average loss of internal energy in a single dissociation event. This step is important for development of reduced order models of aerothermochemistry. The coupling coefficient, $C_{x,i}$, where $x$ denotes the vibrational, rotational or rovibrational mode, can be defined for each internal state as well as for the entire vibrational or rotational manifold. The state-specific coupling coefficient is estimated as follows

$$C_{x,i} = \frac{D_i n_{O_2} n_i^{eq} \left(\rho_O^2 - \rho_i\right) e_{x,i}}{\sum_i D_i n_{O_2} n_i^{eq} \left(\rho_O^2 - \rho_i\right)} \tag{15}$$

where $e_{x,i}$ stands for the corresponding internal energy and $D_i$ is the state-specific dissociation rate coefficient. The summation of $C_{x,i}$ over the entire rovibrational ladder produces the average coupling coefficient $C_x$ that

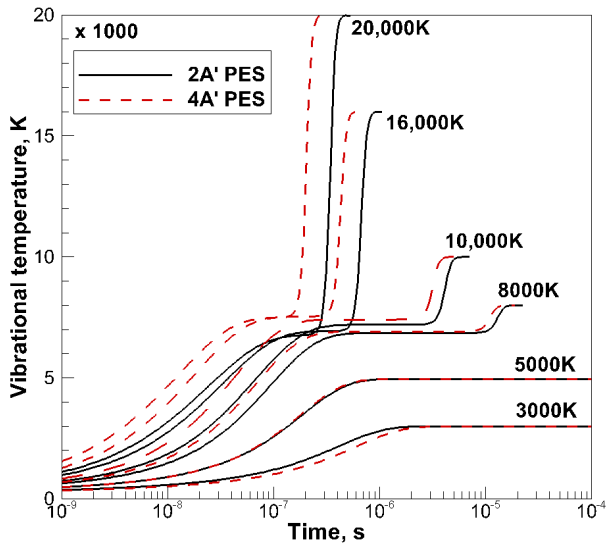


Fig. 15: Thermalization of vibrational mode assuming rotational equilibrium

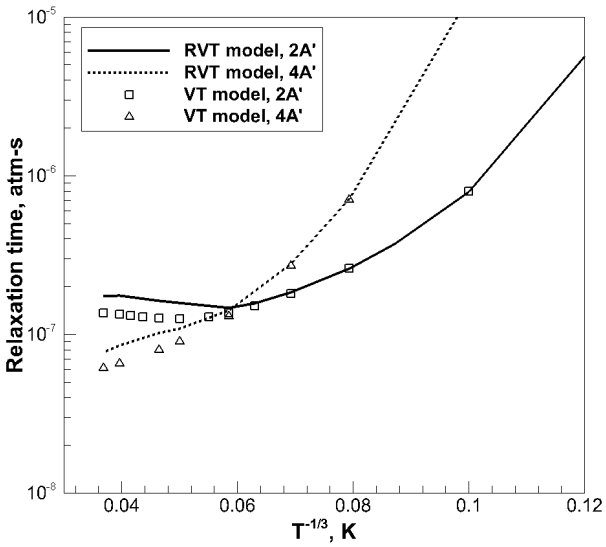


Fig. 16: Vibrational relaxation times, VT and RVT thermodynamic model

can be utilized in the formulation of a vibrational energy equation in multi-temperature models [26]. In the present work, the energy rate coefficients, given by Eq. (15), are normalized by the classical dissociation energy $D_e$ of oxygen.

The average loss of internal, vibrational and rotational energies is shown in Fig. 17a for 2A′ and 4A′ PES by curves with square and triangular symbols. The differences in the PES topology weakly influence the removal of rotational energy in the range of temperatures between 3000 and 20,000 K. The influence of the particular PES on the loss of vibrational energy is more pronounced. The low-lying 2A′ potential energy surface with the lower barrier and deeper potential minimum suggests smaller loss of vibrational, and, consequently, the internal energy, compared to that in the 4A′ PES in the entire temperature range. This difference is largest at $T$=3000 K, i.e. at conditions when the influence of potential barrier is significant.

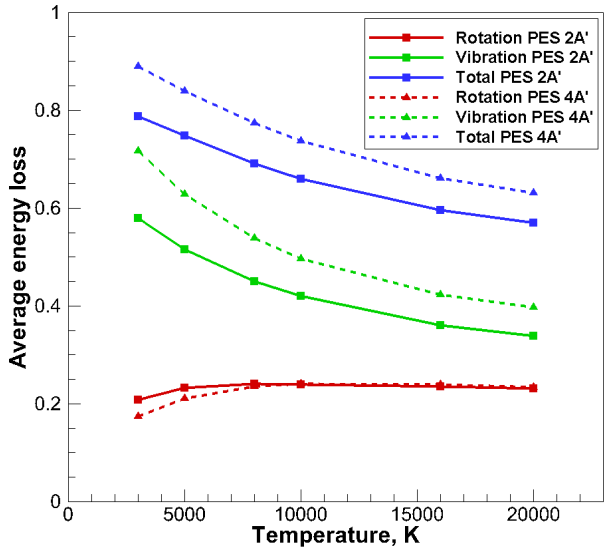


(a) $O_2$–N collisions, 2A′ and 4A′ PESs

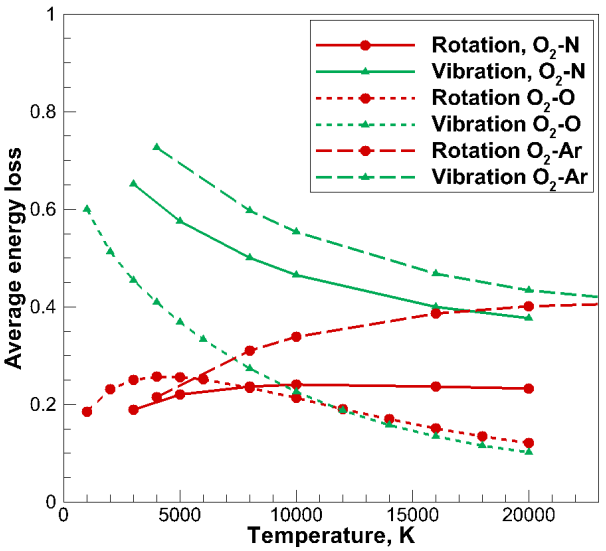


(b) $O_2$–X collisions, where X is N, Ar and O

Fig. 17: Energy loss coefficients due to dissociation

The overview of available $C_{rot}$ and $C_{vib}$ for molecular oxygen in collisions with different projectiles is

given in Fig. 17b. The $O_2$–N, $O_2$–Ar and $O_2$–O systems are shown with solid, dashed and dashed-dotted lines, respectively. The $O_2$–O data [21] represents the energy loss coefficients in the presence of a strongly attractive, barrierless potential [27]. On the contrary, the $O_2$–Ar data [22] is obtained assuming a purely repulsive Buckingham potential [28]. The $O_2$–N energy loss coefficients are obtained by concurrent master equation simulations using rates from the 2A′ and 4A′ PESs and their statistical weights.

Among the considered projectiles, the $O_2$–O interaction has the smallest coupling coefficient $C_{vib}$ and the most rapid decrease of $C_{vib}$ with temperature. As discussed previously [21], this is the effect of the barrierless potential energy surface. Dissociation rate coefficient in $O_2$–O collisions rapidly increases with translational temperature, while the vibrational relaxation time has a weak temperature dependence. This results in the incomplete thermalization before the onset of dissociation at high temperatures. The vibration-dissociation coupling coefficient for $O_2$–N system is smaller than that in the $O_2$–Ar collisions and has a similar temperature dependence.

The temperature dependence of $C_{rot}$ for $O_2$–O and $O_2$–N significantly differs from that in $O_2$–Ar. The latter rapidly increases with temperature, approaching $C_{vib}$. This is explained by a large contribution of rotational states with high energies (particular, quasi-bound states) in the process of dissociation. On the contrary, the $O_2$–O and $O_2$–N systems have a relatively small $C_{rot}$, indicating the limited influence of highly excited rotational states. The state-specific and cumulative $O_2$–N $C_{vib}$ and $C_{rot}$ are shown in Fig. 18 for a temperature of 10,000 K. Cumulative coefficients are normalized to their own maximum value. While the relative contribution of states into the integral value of energy rate coefficient is nearly the same for both the 2A′ and 4A′ PESs, the absolute contribution of quasi-bound states into $C_{rot}$ and $C_{vib}$ is higher for the 4A′ PES. In other words, pre-dissociated states have a more pronounced influence on the dissociation process in the case of repulsive atom-molecule interaction. A similar conclusion about the importance of QB states is drawn in [7] for the $N_2$–N system.

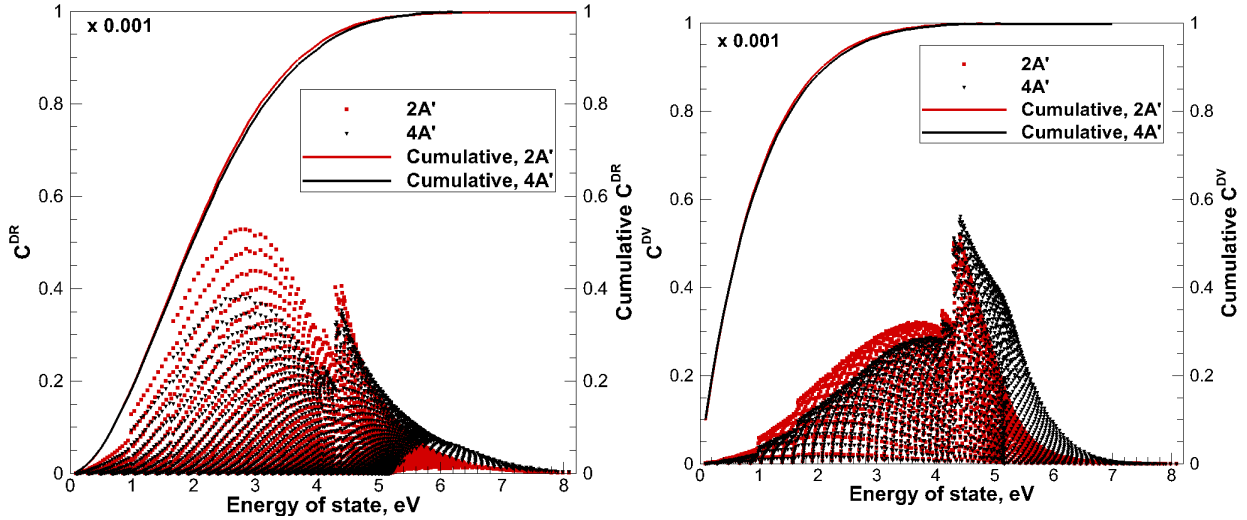


(a) Rotational mode

(b) Vibrational mode

Fig. 18: Quasi-stationary state-specific energy loss coefficients, T=10,000 K

Dissociation rates coefficients, obtained via the master equation simulations on the 2A′ and 4A′ PESs, are shown in Fig. 19. Red line, square and circular symbols correspond to $D$, estimated during the QSS phase on the 2A′, 4A′ and 2A′+4A′ PESs, respectively. Black line, triangular symbols and blue line correspond to the thermal equilibrium dissociation rate, estimated from state-specific QCT data assuming $T=T_{vib}=T_{rot}$. The green line with circular symbols corresponds to dissociation rate proposed by Park [29] and evaluated using the governing temperature $T_a = \sqrt{TT_{vib}}$, where $T_{vib}$ corresponds to vibrational temperature during the QSS phase in Fig. 14. These parameters are shown in Table 1. The column $D_{QSS}$ describes the quasi-steady dissociation rate, from the concurrent solutions of master equations on 2A′ and 4A′ PESs.

Both QSS and thermal equilibrium dissociation rate coefficients are nearly identical for the two lowest $O_2N$ PESs. The quasi-steady dissociation rate coefficient is lower than the equilibrium dissociation rate due to the incomplete thermalization of the rovibrational degrees of freedom. For the entire range of considered

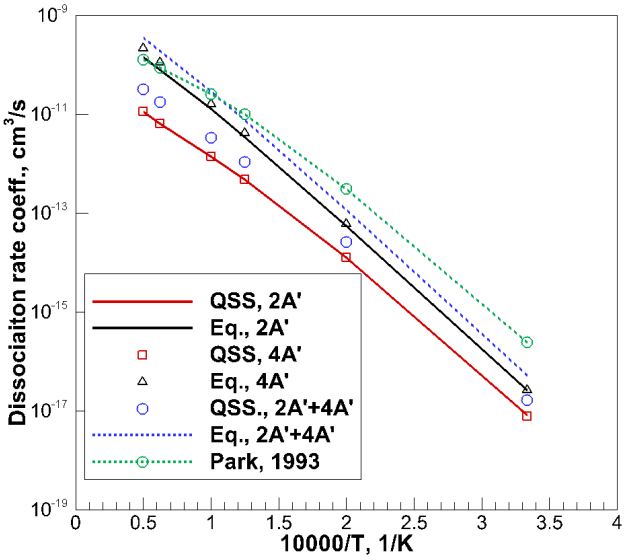


Fig. 19: $O_2$–N quasi-stationary and thermally equilibrium dissociation rates

| T | $T_{vib}$, QSS | $D_{Park}(\sqrt{TT_{vib}})$ | $D_{QSS}$ |
|---|---|---|---|
| 3000 | 3000.0 | 2.461e-16 | 1.636e-17 |
| 5000 | 4965.2 | 3.085e-13 | 2.594e-14 |
| 8000 | 7215.7 | 1.002e-11 | 1.083e-12 |
| 10,000 | 8090.6 | 2.541e-11 | 3.332e-12 |
| 16,000 | 9152.5 | 8.531e-11 | 1.742e-11 |
| 20,000 | 9442.9 | 1.240e-10 | 3.126e-11 |

Table 1: $O_2$–N quasi-stationary and thermally equilibrium dissociation rates

temperatures, Park's rate substantially overestimates the present $D_{QSS}$ by a factor of 4 to 15. Using the values of governing temperature $T_a$ during the QSS phase, it is possible to derive the dissociation rate from the present QCT data, that can be utilized in fluid dynamic computer codes, being coupled to Park's model of vibrationally nonequilibrium dissociation. This rate has the following Arrhenius parameters: A = $1.5\times10^{-6}$ $cm^3/s$, B=-0.6907, C = 59500 K.

## IV. Conclusion

A comprehensive investigation of $O_2$–N collisional dynamics is conducted using the two lowest $2A'$ and $4A'$ *ab-initio* potential energy surfaces. In contrast with previous works in this field, the present paper is dedicated to the study of rovibrational relaxation and dissociation of molecular oxygen. It is found that the $O_2$–N vibrational relaxation time, obtained from the solution of master equations, is noticeably lower than that in $N_2$–O collisions, previously assumed as a substitute for the $O_2$–N molecular system.

The $2A'$ potential energy surface is found to demonstrate strong attractive properties, leading to a significantly faster vibrational relaxation at low temperatures, compared to the $4A'$ PES. The thermalization of the rotational mode is studied in the present paper as well. Both the $2A'$ and $4A'$ PESs produce similar rotational relaxation times in the wide range of temperatures observed in hypersonic flows. The solution of master equations indicates the presence of rotational nonequilibrium in $O_2$–N collisions at temperatures above 8000 K. This fact should be considered when simulating shock flows during re-entry of spacecraft or cruise flight of hypersonic vehicle. At high temperatures, the rotational relaxation becomes faster than the vibrational relaxation. A possible explanation of this phenomenon is that the $O_2$–N exchange channel leads to products other than initial species, and, thus, does not contribute in the $O_2$ relaxation mechanism.

Quasi-steady and thermal equilibrium dissociation rate coefficients are reported in the temperature interval between 3000 and 20,000 K. It is shown that the $O_2$ depletion proceeds with a similar rate on the 2A′ and 4A′ PESs. The QSS dissociation rate coefficient is found to be lower than the previously assumed data by a factor between 4 and 15. Arrhenius parameters for the new QSS dissociation rate are proposed using Park's multi-temperature model and the values of quasi-steady vibrational temperature obtained from the solution of master equations. Since the validity of the QSS assumption is questionable at translational temperatures higher than 10,000 K, one should use this curve-fitted data with caution.

Finally, the relaxation-dissociation coupling coefficients, that describe the loss of internal energy due to dissociation, are derived. The present $O_2$–N vibrational energy rate coefficients take an intermediate value between those for the $O_2$–Ar and $O_2$–O systems. The $O_2$–N rotational energy rate coefficient exhibits a behavior similar to $O_2$–O. The absolute value of $C_{rot}$ in $O_2$–N collisions is substantially lower than in $O_2$–Ar collisions. For this reason, it is possible to speak about the relative unimportance of highly excited rotational and quasi-bound states in the process of dissociation.



## Acknowledgments

The authors gratefully acknowledge funding for this work through Air Force Office of Scientific Research Grant FA9550-12-1-0483.

## References

[1]Y. Zeldovich, D. Frank-Kamenetskii, and P. Sadovnikov, *Oxidation of nitrogen in combustion.* Publishing House of the Acad of Sciences of USSR, 1947.

[2]M. E. Whitson, L. A. Darnton, and R. J. McNeal, "Vibrational energy distribution in the NO produced by the reaction of N($^4$S) with $O_2$," *Chemical Physics Letters*, vol. 41, no. 3, pp. 552–556, 1976.

[3]A. Rahbee and J. Gibson, "Rate constants for formation of NO in vibrational levels v = 2 through 7 from the reaction N($^4$S)+ $O_2 \rightarrow$ NO+O," *Journal of Chemical Physics*, vol. 74, no. 9, pp. 5143–5148, 1981.

[4]D. Bose and G. V. Candler, "Thermal rate constants of the $O_2$+ N $\rightarrow$ NO + O reaction based on the 2A′ and 4A′ potential-energy surfaces," *Journal of Chemical Physics*, vol. 107, no. 16, pp. 6136–6145, 1997.

[5]R. L. Jaffe, M. D. Pattengill, and D. W. Schwenke, "Classical trajectory studies of gas phase reaction dynamics and kinetics using ab initio potential energy surfaces," in *Supercomputer Algorithms for Reactivity, Dynamics and Kinetics of Small Molecules*, pp. 367–382, Springer, 1989.

[6]J. Livesey, A. Roberts, and A. Williams, "The formation of oxides of nitrogen in some oxy-propane flames," *Combustion Science and Technology*, vol. 4, no. 1, pp. 9–15, 1971.

[7]M. Panesi, R. L. Jaffe, D. W. Schwenke, and T. E. Magin, "Rovibrational internal energy transfer and dissociation of $N_2$ ($^1\Sigma_g^+$)- N ($4S_u$) system in hypersonic flows," *Journal of Chemical Physics*, vol. 138, no. 4, p. 044312, 2013.

[8]J. G. Kim and I. D. Boyd, "State-resolved master equation analysis of thermochemical nonequilibrium of nitrogen," *Chemical Physics*, vol. 415, pp. 237–246, 2013.

[9]C. Park, "Thermochemical relaxation in shock tunnels," *Journal of Thermophysics and Heat Transfer*, vol. 20, no. 4, pp. 689–698, 2006.

[10]R. Sayós, C. Oliva, and M. González, "New analytical (2A′, 4A′) surfaces and theoretical rate constants for the N($^4$S)+ $O_2$ reaction," *Journal of Chemical Physics*, vol. 117, pp. 670–679, 2002.

[11]R. B. Bernstein, "Atom-molecule collision theory; a guide for the experimentalist," in *Atom-molecule Collision Theory; a Guide for the Experimentalist*, vol. 1, 1979.

[12]D. G. Truhlar and J. T. Muckerman, "Reactive scattering cross sections III: quasiclassical and semiclassical methods," in *Atom-Molecule Collision Theory*, pp. 505–566, Springer, 1979.

[13]M. Gilibert, A. Aguilar, M. González, and R. Sayós, "Quasiclassical trajectory study of the N($^4S_u$)+ $O_2$($^3X\Sigma_g^-$) $\rightarrow$ NO ($X^2\Pi$)+ O ($^3P_g$) atmospheric reaction on the 2 A ground potential energy surface employing an analytical sorbiemurrell potential," *Chemical Physics*, vol. 172, no. 1, pp. 99–115, 1993.

[14]G. Herzberg, *Molecular spectra and molecular structure.* van Nostrand, 1957.

[15]C. Lee and H.-R. Kim, "A classical trajectory study of O + $O_2$ collision," *Chemical Physics Letters*, vol. 233, no. 5, pp. 658–664, 1995.

[16]D. Andrienko and I. D. Boyd, "Investigation of oxygen vibrational relaxation by quasi-classical trajectory method," *Chemical Physics*, vol. 459, pp. 1–13, 2015.

[17]C. Park, "Rotational relaxation of $N_2$ behind a strong shock wave," *Journal of Thermophysics and Heat Transfer*, vol. 18, no. 4, pp. 527–533, 2004.

[18]D. Eckstrom, "Vibrational relaxation of shock-heated $N_2$ by atomic oxygen using the ir tracer method," *Journal of Chemical Physics*, vol. 59, no. 6, pp. 2787–2795, 1973.

[19]R. J. McNeal, M. E. Whitson, and G. R. Cook, "Temperature dependence of the quenching of vibrationally excited nitrogen by atomic oxygen," *Journal of Geophysical Research*, vol. 79, no. 10, pp. 1527–1531, 1974.

[20]W. Breshears and P. Bird, "Effect of oxygen atoms on the vibrational relaxation of nitrogen," *Journal of Chemical Physics*, vol. 48, no. 10, pp. 4768–4773, 1968.

[21]D. A. Andrienko and I. D. Boyd, "High fidelity modeling of thermal relaxation and dissociation of oxygen," *Physics of Fluids*, vol. 27, no. 11, p. 116101, 2015.

[22]J. G. Kim and I. D. Boyd, "Thermochemical nonequilibirum modeling of electronically excited molecular oxygen," in *11th AIAA/ASME Joint Thermophysics and Heat Transfer Conference*, AIAA paper 2014-2963, 2014.

[23]M. Quack and J. Troe, "Complex formation in reactive and inelastic scattering: Statistical adiabatic channel model of unimolecular processes III," *Berichte der Bunsengesellschaft für physikalische Chemie*, vol. 79, no. 2, pp. 170–183, 1975.

[24]C. Park, *Nonequilibrium hypersonic aerothermodynamics*. Wiley, 1989.

[25]P. V. Marrone and C. E. Treanor, "Chemical relaxation with preferential dissociation from excited vibrational levels," *Physics of Fluids*, vol. 6, no. 9, pp. 1215–1221, 1963.

[26]P. A. Gnoffo, R. N. Gupta, and J. L. Shinn, "Conservation equations and physical models for hypersonic air flows in thermal and chemical nonequilibrium," Tech. Rep. NASA Technical Paper 2867, National Aeronautics and Space Administration, Office of Management, Scientific and Technical Information Division Washington, DC, 1989.

[27]A. Varandas and A. Pais, "A realistic double many-body expansion (DMBE) potential energy surface for ground-state $O_3$ from a multiproperty fit to ab initio calculations, and to experimental spectroscopic, inelastic scattering, and kinetic isotope thermal rate data," *Molecular Physics*, vol. 65, pp. 843–860, Nov 1988.

[28]A. Gross and G. D. Billing, "Rate constants for ozone formation," *Chemical Physics*, vol. 187, no. 3, pp. 329–335, 1994.

[29]C. Park, "Review of chemical-kinetic problems of future nasa missions. I - Earth entries," *Journal of Thermophysics and Heat Transfer*, vol. 7, pp. 385–398, Jan 1993.